Growth of rough-surface p-GaN layers on InGaN/GaN multiple-quantum-well structures by metalorganic chemical vapor deposition and their application to GaN-based solar cells

Takuma Mori[1], Takashi Egawa[1,2] and Makoto Miyoshi[1,2*)]

[1]*Research Center for Nano Devices and Advanced Materials, Nagoya Institute of Technology, Nagoya 466-8555, Japan*

[2]*Innovation Center for Multi-Business of Nitride Semiconductors, Nagoya Institute of Technology, Nagoya 466-8555, Japan*

We conducted the study on the growth of rough-surface p-GaN layers on InGaN/GaN multiple-quantum-well (MQW) structures by metalorganic chemical vapor deposition (MOCVD). It was found that the sum of InGaN well thickness t_{well_total} was a predominant factor to form the rough surface, in addition to the growth temperature as low as 800°C for the p-GaN layers. Microstructure analyses revealed that the rough surfaces consisted of a certain number of hexagonal V-shaped pits starting from dislocations propagated through an under layer and they increased with the increased t_{well_total}. It was confirmed that the light absorption was enlarged for MQW structure samples with rough-surface p-GaN layers on the top, owing to not only the thickness effect in MQWs but also their reduced light reflection on the surfaces. It was also confirmed that these optical properties contributed to the performance improvement in InGaN/GaN MQW solar cells.

---

* Corresponding author:

E-mail address: miyoshi.makoto@nitech.ac.jp (Makoto Miyoshi)

Keywords: InGaN/GaN; Solar cell; MQW; Well thickness

1. Introduction

In addition to visible and ultraviolet light-emitting devices, InGaN alloys have recently been viewed as a promising candidate for solar cell materials, owing to their nontoxicity and the direct-transition and variable bandgaps [1-15]. The InGaN-based solar cells are expected to exhibit energy conversion efficiencies (ECE) larger than 50% by forming multijunction tandem cells similar to other III-V compound semiconductor solar cells [16]. However, it is known to be difficult to grow thick InGaN layers with sufficient crystal quality owing to their thermodynamic instability [17-20]. Until now, therefore, for realizing the InGaN-based solar cells, many researchers have focused on multiple-quantum-well (MQW) structures containing a number of thin InGaN well layers [6-15]. This is because the MQW structures can pseudomorphically realize the thick InGaN layers with less difficulty during the material growth. Recently, Wu *et al* have reported that a rough-surface p-GaN layer can be grown at a temperature as low as approximately 800°C on an InGaN/GaN MQW structure by metalorganic chemical vapor deposition (MOCVD) [21]. When it comes to light-emitting diodes (LEDs), it has also been reported that the light extraction efficiency was improved by employing the as-grown rough-surface p-GaN layer on the top [21-23]. In the same way as LEDs, if the electrical characteristics were not impaired, it could be considered that the top p-GaN layers with a rough surface improve the solar cell performance because they can increase the light absorption by reducing the light reflection of the device surfaces. Up to now, however, there have been only a few reports focusing on the application of as-grown rough surfaces to the InGaN-based solar cells [3-4]. Moreover, details on conditions for forming the rough surfaces have not been clarified. To control over the surface morphology of as-grown films, it must be important to figure out the effective factors in the material growth and stacking structures. In this study, therefore, to consider the application of MOCVD-grown rough-surface p-GaN layers to InGaN/GaN MQW solar cells, their underlying MQW structures and growth conditions were

investigated. Then, to understand the mechanism of the rough surface formation, microstructure observation was carried out. Finally, the effect of the rough surfaces on solar cell performance was studied and discussed.

2. Experimental

Figure 1 shows a schematic of the InGaN/GaN MQW solar cell employed in this study. The solar cell structures were grown on *c*-face sapphire substrates using a horizontal MOCVD system. Here, trimethylgallium (TMG) and trimethylindium (TMI) were used as group-III sources, and NH_3, SiH_4 and Cp_2Mg were used for a nitrogen source, n-type and p-type dopant sources, respectively. As for the MOCVD growth, the substrates were first treated in H_2 flow at 1180°C, and the temperature was then reduced to 500°C for the growth of a 30-nm-thick GaN low-temperature buffer layer. Then, after the growth of a 3-μm-thick n-type GaN contact layer with a Si concentration of approximately $3 \times 10^{18}/cm^3$ at 1160°C, the temperature was reduced again to 800°C for the growth of an InGaN/GaN MQW structures and a p-type contact layer. In this study, the InGaN/GaN MQW structures and the growth conditions for the top p-GaN layers were treated as experimental variables. The MQW structures were characterized using cross-sectional transmission electron microscopy (TEM) and high-resolution X-ray diffraction (HR-XRD) analyses, in the same way as in our previous study [24]. The structural characterization confirmed that the indium contents *x* in the $In_xGa_{1-x}N$ well layers were within 0.10 ± 0.02 and the thickness fluctuation of the InGaN well and GaN barrier layers were within ± 0.6 nm for all samples. The top p-GaN layers were grown by estimating a constant layer thickness of approximately 200 nm from their growth rate. The surface morphology and cross-sectional microstructure were analyzed using the atomic force microscope (AFM) and cross-sectional TEM observations, respectively. The light reflection and transmission spectra were obtained using a UV-visible/NIR spectrophotometer (Hitachi

High-Tech Science, UH4150), from which the light absorption spectra were also derived.

Solar cell devices with a light-receiving area of 1 × 1 mm^2 were fabricated using the conventional photolithographic lift-off method. Here, n-type contact regions were first etched down by BCl_3 plasma reactive ion etching. Next, samples were annealed at 600°C in a nitrogen atmosphere for 25 min to activate the Mg acceptors. Then, n-type contact metals were formed by the electron beam (EB) evaporation of Ti/Al/Ni/Au (15/60/12/60 nm), which were subsequently annealed at 700°C in a nitrogen atmosphere for 30 s. Then, a Ni/Au (5/60 nm) finger-shaped pattern was formed on the p-GaN surface by EB evaporation. Subsequently, samples were subjected to an annealing process at 600°C in an oxygen atmosphere for 5 min to obtain p-type ohmic contacts. Then, the Al_2O_3 film was deposited at 300°C and 0.35 Pa using a Cambridge Nano-tech atomic layer deposition (ALD) system with H_2O and O_3 as oxygen precursors and trimethyl aluminum as an aluminum precursor [25]. Finally, pad electrode patterns were formed by the EB evaporation of Ni/Au (5/60 nm) on the p- and n-type contact metals via through holes of the Al_2O_3 film. The EQE of the fabricated solar cells was evaluated using a spectral response measurement system (Bunkokeiki Co., Ltd.). The ECE and other solar cell properties were evaluated by current–voltage (*I–V*) measurements under an illumination of a 1-sun-power-density (100 mW/cm^2) artificial solar light with a standard air-mass 1.5 global (AM1.5G) spectrum.

3. Results and discussion

3.1. Influence of InGaN/GaN MQW structures on the top p-GaN surface roughness

Table I summarizes the relationship between the InGaN/GaN MQW structures and the measured route mean square (RMS) roughness of the top p-GaN layers, where the p-GaN layers were grown to have a Mg concentration of 5 × $10^{19}/cm^3$ under constant conditions with an input V/III gas ratio of approximately 2,570 and a TMG flow rate of 69.3 μmol/min.

Using these data, we attempted to analyze the influence of the MQW structures on the top p-GaN surface morphology. Figure 2(a) reorganizes the data by focusing the whole MQW thickness t_{MQW_total}, which is the sum of the well and barrier layer thicknesses. As obvious in this figure, the RMS surface roughness abruptly increased at the t_{MQW_total} of around 200 nm and then it almost saturated at an RMS roughness of around 75 nm. On the other hand, Figures 2(b) shows the t_{well_total} dependence of the RMS roughness. Overall, the result indicates a tendency that the RMS surface roughness increased with the increase in t_{well_total}. This means that the RMS roughness increases depending on the thickness or the number of the InGaN well layers. As a result, the t_{MQW_total} or the t_{well_total} seemed to be predominant factors influencing the top p-GaN surface morphologies.

Figures 2(a) and 2(b) also show bird's-eye-view AFM images for typical samples A, B, and C. From the AFM images, it was observed that the top p-GaN layers have flat areas and some hexagonal V-shaped pits on their surfaces, especially when the RMS roughness is as small as in samples A or B. In contrast to this, when the RMS roughness increased as seen in sample C, the number and/or the area occupancy of the V-pits obviously increased and then the flat areas remarkably disappeared. To understand how the V-pits was formed on the surfaces, TEM analyses were carried out. Figures 3(a), 3(b) and 3(c) show cross sectional dark field TEM images for samples A, B, and C taken with a *g*-vector parallel to $[11\bar{2}0]$ direction, in which the pure edge and edge/screw-mixed dislocations are accentuated. In these figures, the corresponding surface AFM images shown in Figure 2 are also inserted as a help in understanding. As Figure 3(a) shows, when the t_{well_total} is small, the V-pits generate from the endpoints of threading dislocations propagated through the n-GaN layer at around a boundary between the InGaN/GaN MQWs and top p-GaN layers. This seems to be consistent with the general tendency for the surface V-pits often seen in many III-nitride heterostructures. When the t_{well_total} increased, as seen in Figure 3(b) and 3(c), the origination

points of the V-pits obviously penetrate down into the MQWs. Further, as seen in Figure 3(c), it was observed that some V-pits starting from the same origination points form a pyramidal surface. Generally, the progress of the lateral growth in nitride crystals strongly depends on the growth temperature. Thus, we consider that the lateral growth of the top p-GaN layers did not progress to cover the hexagonal V-pits, vestiges of the threading dislocations, owing to their low growth temperature.

3.2. Influence of p-GaN growth conditions on their surfaces

It seems natural to consider that the lateral growth of the top p-GaN layers is an important factor influencing the formation of their rough surfaces. Generally, the progress of the lateral growth in GaN films depends on the input V/III gas ratio as well as the growth temperature. Furthermore, we consider the possibility that the Cp_2Mg flow rate might influence on their surfaces as well. Therefore, we investigated the effect of the input V/III gas ratio and Cp_2Mg flow rate on the top p-GaN surface morphology. For the former experiment, the input V/III gas ratio was varied from 1,280 to 10,300 by changing the TMG flow rate from 138.6 to 17.3 μmol/min at a constant NH_3 flow rate of 178,460 μmol/min, where the Cp_2Mg flow rate was also changed in proportion to the TMG flow rate for achieving a constant Mg concentration of approximately $5 \times 10^{19}/cm^3$. In the latter experiment investigating the influence of the Cp_2Mg flow, its flow late was changed from 0 to 0.310 μmol/min under a constant TMG flow rate of 69.3 μmol/min. In the experiments of this section, the MQW structure was maintained at the same structure as sample C seen in the previous section. Figures 4(a) and 4(b) show the variation of the RMS roughness of the p-GaN layers with the input V/III gas ratios and Cp_2Mg flow rates, respectively. The figures also show bird's-eye-view AFM images for typical samples. As seen in Figure 4(a), the RMS surface roughness of the top p-GaN layers showed a decreasing tendency with the increase in the input V/III gas ratio. At the same time, it was

also observed that the edge of the V-pits became smooth to some degree. This is probably because the lateral growth of p-GaN layers was promoted by increasing the input V/III gas ratio. However, even a sample grown under the largest V/III gas ratio of over 10000 also showed an RMS surface roughness as large as over 30 nm. On the other hand, from Figure 4(b), the RMS surface roughness of the top p-GaN layers showed somewhat a decreasing tendency with the decrease in the Cp_2Mg flow rates. Further, it was also observed that the edge of the V-pits became smooth to some degree. These indicate that the lateral growth of p-GaN layers might have been influenced by the Cp_2Mg flow rate to some degree. However, even a sample grown without Cp_2Mg flowing also showed a RMS surface roughness as large as approximately 40 nm. From these, it was concluded that the growth temperature of 800°C was low enough so as not able to form smooth GaN surfaces by covering the V-pits.

3.3. Optical properties of rough-surface p-GaN layers and their application to InGaN/GaN MQW solar cells

To consider the application of the rough surface p-GaN layers to soral cell devices, the light reflection and absorption spectra were measured for typical samples singled out of Table 1: Sample A with a small RMS roughness, sample B with a middle RMS roughness, and sample C with a large RMS roughness. The results are shown in Figures 5(a) and 5(b). As seen in Figure 5(a), it was confirmed that the light absorption was reduced across a wide wavelength range with the increased surface roughness. Further, Figure 5(b) shows that the light absorption in the wavelength range of 365 nm to 480 nm obviously increased when the surface roughness increased. The light absorption in this range is attributed to the InGaN well layers, and therefore its increase seems to be largely due to the increase in t_{well_total}. In addition to this, we also speculate that the reduced light reflection with the rough surfaces largely contributed to the increase in the light absorption. From figure 5(a), on the other hand, it was found that

the amplitude of the vibration ranging from 375nm to 500nm decreases with the increase in RMS roughness. This indicates that the interference of light was weakened for the rough-surface samples. Here, the rough surface would have weakened the light reflected on the surface. In addition, the interface quality or structural fluctuation in the MQW region might have been varied in relation to the surface roughness.

The solar cell devices were fabricated using samples A, B, and C, and their EQE spectra and *I–V* characteristics were evaluated. Figure 6 shows the EQE spectra for the fabricated solar cells. For comparison, Figure 6 also plots the light absorption spectra shown in Figures 5(a) as dashed lines. From this, it is clear that the EQE curves are fairly close to their light absorption curves, especially in the wavelength range of 365 nm to 480 nm corresponding to the InGaN well layers. This indicates high internal quantum efficiencies were achieved for those samples. As a result, a high EQE value of over 80% was observed for sample C. This is explained by not only the thickness effect of InGaN wells but also their reduced light reflection. Figure 7 shows the typical *I–V* characteristics for solar cells fabricated using samples A, B, and C, which were measured under a 1-sun-intensity artificial solar light illumination with an AM1.5G spectrum. Correspondingly, Table II summarizes the basic solar cell characteristics determined from the results shown in Figure 7, which includes the short circuit current density (I_{SC}), open circuit voltage (V_{OC}), fill factor (FF), and ECE. Overall, the evaluation results indicate that ECE varied along with the variation of EQE. This seems to be reasonable because the I_{SC} of solar cells is commonly determined by EQE. Here, we understand that EQE includes the effect of the light reflection reduced with the enlarged surface roughness, as discussed before. From table II, it was also found that the FF tends to decrease with the increase in RMS surface roughness. One thing is, the shunt resistance might was reduced for the rough-surface samples. That is, the surface roughness might be related to the interface quality in the MQW structures including the p-GaN top layers. However, it should

be noted that the fabricated solar cells did not show any deteriorated *I–V* characteristics even for sample C with the largest RMS roughness. This implies that the rough-surface p-GaN did not affect the diode characteristics so much. As a result, sample C with the largest t_{well_total} exhibited the highest ECE of approximately 1.3% in this study.

4. conclusion

To consider the application of rough surface p-GaN layers to the InGaN/GaN MQW solar cells, the MQW structures and the growth condition for the top p-GaN layers were carefully investigated. The results indicated that the RMS surface roughness was strongly affected by the sum of InGaN well layers t_{well_total}. The AFM and TEM analyses revealed that the hexagonal V-shaped pits caused the rough surfaces and they increased with increasing t_{well_total}. It was also indicated that a low growth temperature had a large effect for the rough surface formation than their other growth conditions such as the input V/III gas ratio or Cp_2Mg flow rate. The sample with the large t_{well_total} of over 100 nm exhibited high solar cell performance with a high EQE of over 80%, owing to their increased light absorption which was attributed to their reduced light reflection in addition to the increased t_{well_total} itself.

Acknowledgement

This work was partially supported by the Super Cluster Program of the Japan Science and Technology Agency (JST).

[1] Wu J, Walukiewicz W, Yu K M, Shan W, Ager II J W, Haller E E, Lu H, Schaff W J, Metzger W K and Kurtz S 2003 J. Appl. Phys. **94** 6477–82

[2] Jani O, Ferguson I, Honsberg C and Kurtz S 2007 Appl. Phys. Lett. **91** 132117

[3] Matioli E, Neufeld C, Iza M, Cruz S C, Al-Heji A A, Chen X, Farrell R M, Keller S, DenBaars S, Mishra U, Nakamura S, Speck J and Weisbuch C 2011 Appl. Phys. Lett. **98** 021102

[4] Farrell RM et al 2011 Appl. Phys. Lett. **98** 201107

[5] Bhuiyan AG, Sugita K, Hashimoto A and Yamamoto A 2012 IEEE J. Photovolt. **2** 276–93

[6] Dahal R, Pantha B, Li J, Lin JY and Jiang HX 2009 Appl. Phys. Lett. **94** 063505

[7] Young NG et al 2013 Appl. Phys. Lett. **103** 173903

[8] Young NG et al 2014 Appl. Phys. Lett. **104** 163902

[9] Wierer Jr JJ, Koleske DD and Lee SR 2012 Appl. Phys. Lett. **100** 111119

[10] Watanabe N, Yokoyama H, Shigekawa N, Sugita K and Yamamoto A 2012 Japan. J. Appl. Phys. **51** 10ND10

[11] Watanabe N, Mitsuhara M, Yokoyama H, Liang J and Shigekawa N 2014 Japan. J. Appl. Phys. **53** 112301

[12] Redaelli L et al 2015 Japan. J. Appl. Phys. **54** 072302

[13] Redaelli L et al 2014 Appl. Phys. Lett. **105** 131105

[14] Valdueza-Felip S et al 2013 Japan. J. Appl. Phys. **52** 08JH05

[15] Lee S, Honda Y and Amano H 2016 J. Phys. D: Appl. Phys. **49** 025103

[16] Takamoto T, Washio H and Juso H 2014 In. Proc. IEEE photovoltaic specialist conf. 1-5

[17] Thaler GT, Koleske DD, Lee SR, Bogart KHA and Crawford MH 2010 J. Cryst. Growth **312** 1817–22

[18] Nagamoto T, Kuboyama T, Minamino H and Omoto O 1989 Japan J. Appl. Phys. **28** L1334–6

[19] Yoshimoto N, Matsuoka T, Sasaki T and Katsui A 1991 Appl. Phys. Lett. **59** 2251–3

[20] Tran CA et al 1998 J. Cryst. Growth **195** 397–400

[21] Wu LW et al 2003 Solid-State Electronics **47** 2027-30

[22] Tsai CM, Sheu JK, Lai WC, Hsu YP, Wang PT, Kuo CW, Chang SJ and Su YK 2005 IEEE electron device letters **26** 464-6

[23] Lai FI, Hsieh YL and Lin WT 2011 Diamond and Related Materials **20** 770-3

[24] Miyoshi M, Tsutsumi T, Kabata T, Mori T and Egawa T 2017 Solid-State Electronics **129** 29-34

[25] Kubo T, Freedsman JJ, Iwata Y and Egawa T 2014 Semicond. Sci. Technol. **29** 045004

Table I: Structural characterization results for MOCVD-grown InGaN/GaN MQW solar cell structures. Here, t_{well} and $t_{barrier}$ are the average thicknesses of the InGaN well and GaN barrier layers, respectively, and n_{well} are the number of InGaN well layers, respectively. Further, t_{well_total} is the sum total of the InGaN well layer thickness. The plus/minus signs represent thickness fluctuations of the respective stacking layers. RMS roughness was obtained by AFM surface analyses.

Sample ID	t_{well}	$t_{barrier}$	n_{well}	t_{well_total}	RMS roughness
A	1.0 ± 0.6 nm	5.5 ± 0.6 nm	27	27.0 nm	37.8 nm
B	3.2 ± 0.6 nm	5.5 ± 0.6 nm	22	70.4 nm	58.4 nm
C	3.2 ± 0.6 nm	4.0 ± 0.6 nm	36	115.2 nm	69.6 nm
D	6.0 ± 0.6 nm	5.5 ± 0.6 nm	16	96.0 nm	66.9 nm
E	3.2 ± 0.6 nm	4.0 ± 0.6 nm	47	150.4 nm	75.3 nm
F	3.2 ± 0.6 nm	4.0 ± 0.6 nm	24	76.8 nm	20.4 nm
G	3.2 ± 0.6 nm	5.5 ± 0.6 nm	32	102.4 nm	72.0 nm

Table II: Summary of fabricated solar cells including short circuit current density (I_{SC}), open circuit voltage (V_{OC}), fill factor (FF), and energy conversion efficiency (ECE).

Sample ID	t_{well_total}	RMS roughness	I_{SC} (mA/cm^2)	V_{OC} (V)	FF	ECE (%)
A	27 nm	37.8 nm	0.25	2.03	0.701	0.36
B	66 nm	58.4 nm	0.88	1.98	0.606	1.06
C	108 nm	69.6 nm	1.34	1.71	0.572	1.31

Figure captions

Figure 1. Schematic of InGaN/GaN MQW solar cells

Figure 2. The relationship between the RMS surface roughness between the sum of the well layer thicknesses t_{well_total}, where bird's-eye-view AFM images for typical samples A, B, and C are also shown.

Figure 3. Cross sectional dark field TEM images for samples A, B, and C, which were taken with a *g*-vector parallel to $[11\bar{2}0]$ direction so that pure edge dislocations and edge/screw-mixed dislocations can be observed. AFM images are the same as given in Figure 2.

Figure 4. The variation of the RMS surface roughness of p-GaN layers with (a) the input V/III gas ratios and (b) the Cp_2Mg flow rates, respectively. Bird's-eye-view AFM images for typical samples are also shown.

Figure 5. (a) Light reflection and (b) light absorption spectra for samples A, B, and C with the different MQW structures and surface roughness.

Figure 6. EQE spectra for samples A, B, and C with the different MQW structures and surface roughness. For comparison, the light absorption spectra shown in Figures 5(a) are also plotted as dashed lines.

Figure 7. $I-V$ characteristics for samples A, B, and C with the different MQW structures and surface roughness, which were measured under a 1-sun-intensity artificial solar light illumination with an AM1.5G spectrum.

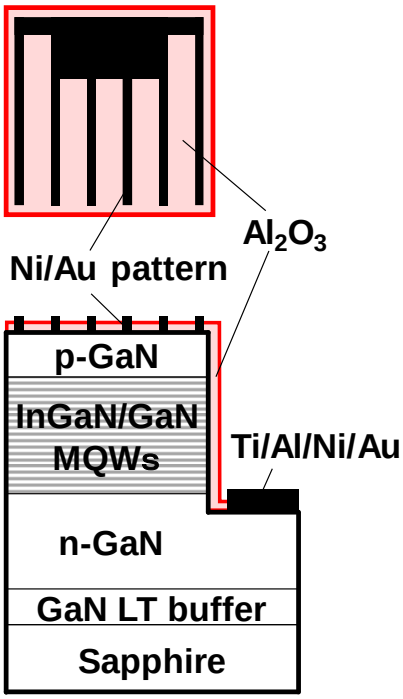
Ni/Au pattern
Al2O3
p-GaN
InGaN/GaN
MQWs
Ti/Al/Ni/Au
n-GaN
GaN LT buffer
Sapphire

Figure 1

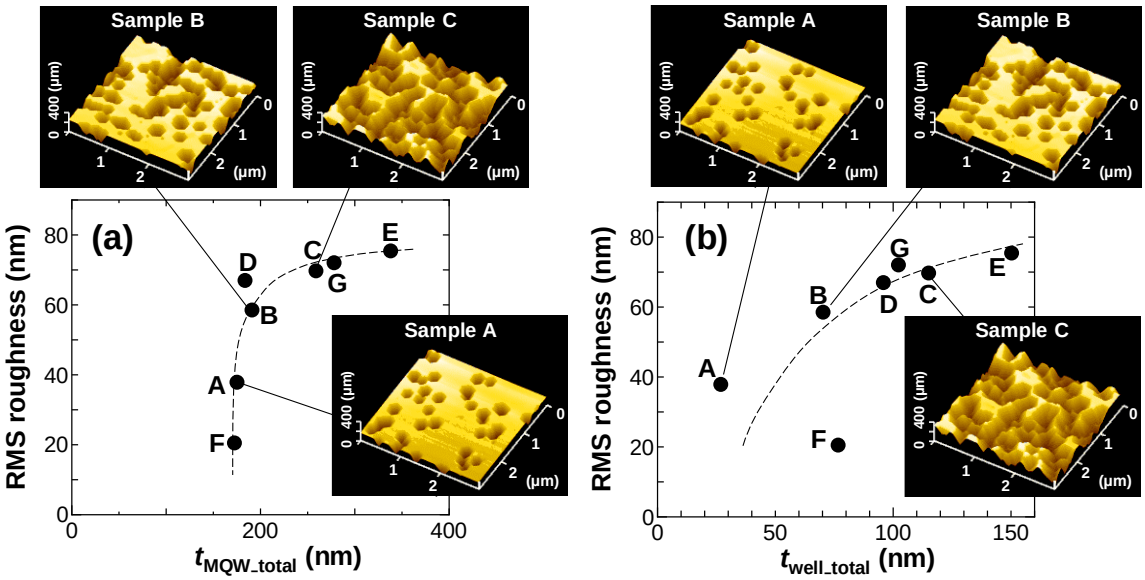
Sample B
Sample C
Sample A
Sample B
(a)
(b)
RMS roughness (nm)
t_{MQW_total} (nm)
t_{well_total} (nm)
A
B
C
D
E
F
G
Sample A
Sample C
(μm)

Figure 2

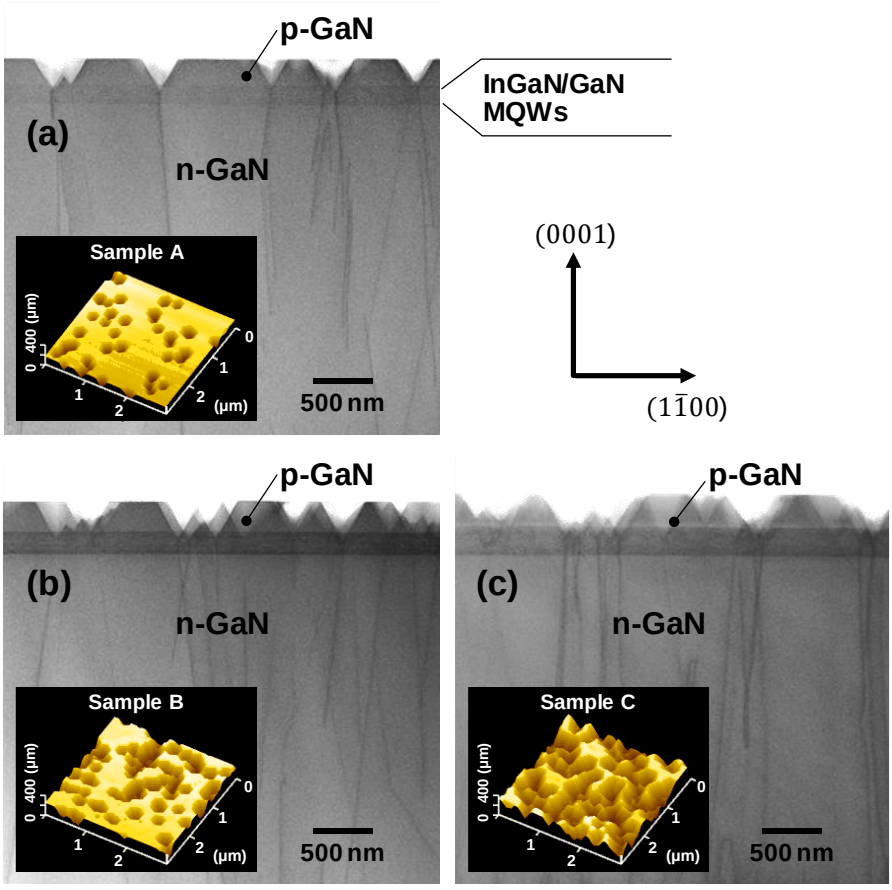
p-GaN
InGaN/GaN
MQWs
(a)
n-GaN
Sample A
0 400 (μm)
0
1
2
(μm)
500 nm
(0001)
(1$\bar{1}$00)
p-GaN
(b)
n-GaN
Sample B
500 nm
p-GaN
(c)
n-GaN
Sample C
500 nm

Figure 3

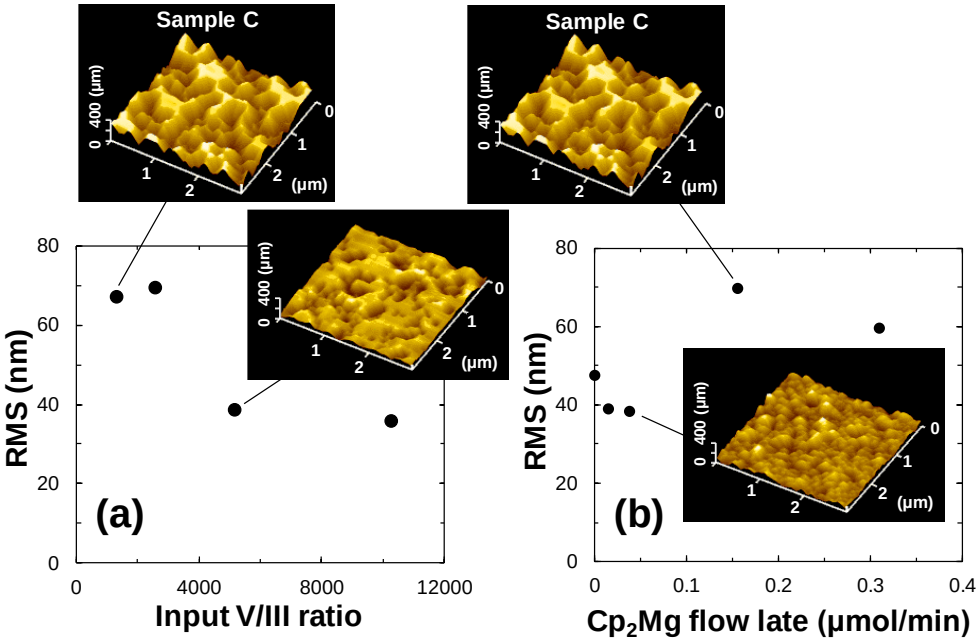
Sample C
Sample C
RMS (nm)
Input V/III ratio
(a)
(b)
Cp2Mg flow late (μmol/min)
(μm)

Figure 4

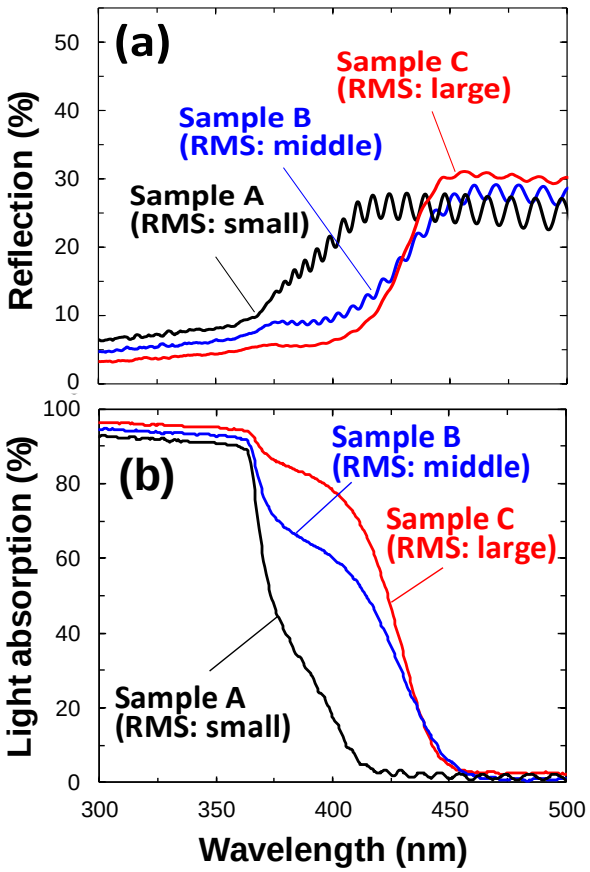
(a)
Sample C
(RMS: large)
Sample B
(RMS: middle)
Sample A
(RMS: small)
Reflection (%)
0
10
20
30
40
50
(b)
Sample B
(RMS: middle)
Sample C
(RMS: large)
Sample A
(RMS: small)
Light absorption (%)
0
20
40
60
80
100
300
350
400
450
500
Wavelength (nm)

Figure 5

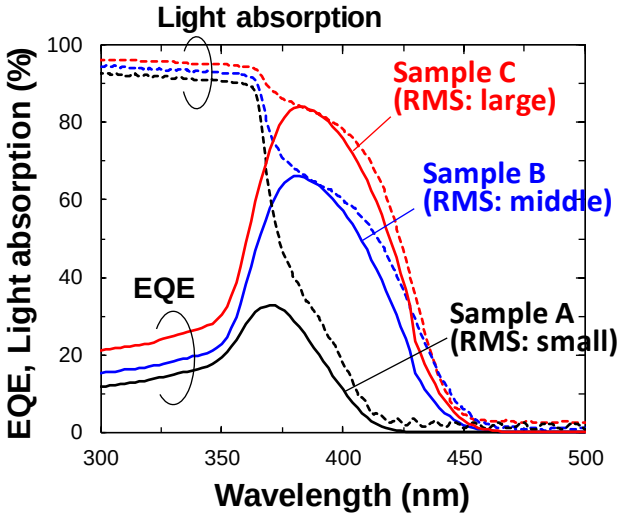
Light absorption
EQE, Light absorption (%)
100
80
60
40
20
0
300
350
400
450
500
Wavelength (nm)
Sample C
(RMS: large)
Sample B
(RMS: middle)
Sample A
(RMS: small)
EQE

Figure 6

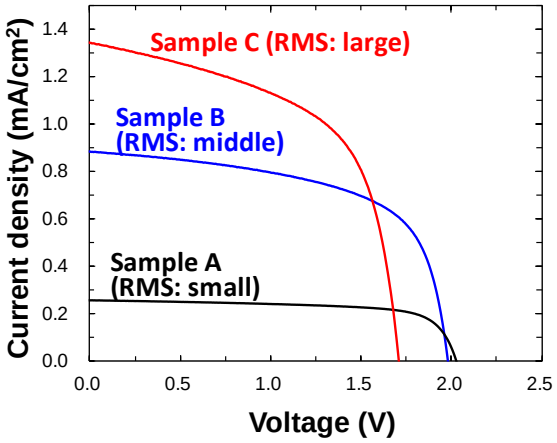
Sample C (RMS: large)
Sample B
(RMS: middle)
Sample A
(RMS: small)
Current density (mA/cm²)
Voltage (V)
0.0
0.2
0.4
0.6
0.8
1.0
1.2
1.4
0.0
0.5
1.0
1.5
2.0
2.5

Figure 7